Journal of Vacuum Science Technology A

Nb – doped TiO_2 Coatings Developed by High Power Impulse Magnetron Sputtering – Chemical Vapour Deposition Hybrid Deposition Process

Running title: Nb – doped TiO_2 depositied by HiPIMS – CVD hybrid method

Running Authors: Kulczyk-Malecka et al.

Justyna Kulczyk-Malecka[1], David Donaghy[2], Brice Delfour-Peyrethon[1], M. Werner[3], Paul R. Chalker[3], James W. Bradley[2], Peter J. Kelly[1, a)]

[1] Surface Engineering Group, Manchester Metropolitan University, Manchester M1 5GD, United Kingdom
[2] Department of Electrical Engineering and Electronics, University of Liverpool, Brownlow Hill, L69 3GJ, United Kingdom
[3] Department of Engineering, University of Liverpool, Liverpool L69 3GH, United Kingdom

[a)] Electronic mail: peter.kelly@mmu.ac.uk

Novel methods for the deposition of thin functional coatings, such as hybrid Physical Vapour Deposition – Chemical Vapour Deposition (PVD – CVD) technologies have the potential to become an important means of overcoming the limitations of current processes, such as low deposition rates, associated with some sputtering processes or limited material/precursor choices, associated with CVD processes. This work explores the potential of addressing these issues through the development of a hybrid system, which combines the latest magnetron sputtering technology, High Power Impulse Magnetron Sputtering (HiPIMS), with Plasma Enhanced Chemical Vapour Deposition (PECVD) technology. This system seeks to overcome the limitations of each technique and provide a new, flexible deposition tool for functional films, such as transparent conductive oxides. In this system, the plasma generated by the magnetron provides a source of electrons to drive the CVD precursor decomposition and reaction chemistry in the PECVD process. Consequently, only one power supply is required.

Thus, niobium – doped titania coatings were deposited on glass and Si wafer substrates by this hybrid HiPIMS – CVD technique. The TiO_2 coatings were deposited by CVD from a titanium

*Corresponding author: peter.kelly@mmu.ac.uk
+44(0)161 247 4643

Journal of Vacuum Science Technology A

(IV) tetraisopropoxide (TTIP) precursor via the vapour drawn method. The HiPIMS process provided not only the source of Nb metal dopant to the functional films, but sustained the low temperature CVD process by supplying energetic plasma particles. Furthermore, since HiPIMS deposition rates are very sensitive to magnetic field strength and the degree of unbalance, by using a magnetron with variable magnetic field strength, it was possible to adjust the dopant content of the film without adjusting the power applied to the magnetron target.

The effect of processing parameters (pulse frequency, peak powers, precursor flow rates, operating pressure, etc.) on generating a stable HiPIMS discharge across the process envelope has been studied. The composition and microstructure of the deposited coatings have been investigated, in respect to variable process parameters, such as substrate temperature and operating pressure.

I. INTRODUCTION

Numerous hybrid deposition systems, in which two or more deposition techniques are carried out simultaneously or sequentially to gain some process advantage, have been developed. Examples include combining magnetron sputtering with pulsed laser deposition; vacuum evaporation and CVD; and pulsed laser deposition with RF discharges [2, 3]. One method that is gaining interest is to combine PVD in the form of magnetron sputtering and plasma enhanced chemical vapour deposition (PECVD) which provides a means to use the advantages of both techniques in a single system.

Magnetron sputtering is a PVD process extensively used in industry for the deposition of functional coatings including many oxides, nitrides and metals in complex multi-layer

stacks with exceptional uniformity of around ±1% over large areas [4]. Dynamic deposition rates on rigid glass or flexible polymeric substrates are, though, in the range of 1 – 10 nm.m/min/kW, which is relatively low and limits throughput, making the deposition of certain materials or products (e.g. many transparent conductive oxides or anti-reflection coatings) uneconomical. In addition, there are still some commercially important materials, such as aluminium oxide, which can cause severe processing instabilities (i.e. arcing, loss of anode surfaces, creation of negative ions, etc.), which restricts their usage.

PECVD [5] is an alternative to PVD. The processes generally have the advantage of very high deposition rates (500 – 2500 nm.m/min/kW), high conformality and low roughness, but are limited, largely by the available precursors, in the range of materials and complexity of the stacks that can be deposited. There are also limitations in uniformity to around ±5 – 10 % due to the nature of the process. Combined magnetron sputtering and plasma-assisted chemistry in a hybrid PVD – CVD system can overcome shortcomings in both techniques.

PVD – CVD hybrid systems can make use of the plasma generated by the magnetron to provide a source of electrons to drive the CVD precursor decomposition and reaction chemistry. Examples of such systems used to deposit functional films include the production of: molybdenum disulfide (MoS_2) – amorphous hydrogenated carbon (a – C:H) composite coatings [6], tantalum nitride-based films [7], hexamethyldisilazane nanocomposites [8], terbium-doped silicon oxide films [9], nanocomposite titanium carbide in an amorphous hydrogenated carbon matrix [10], diamond-like carbon (DLC) films [11-13] and Ti and N co – doped DLC [14].

In a number of sectors, PECVD directly competes with sputtering for market share, with each technology offering different advantages and disadvantages depending on the application (e.g. cost, throughput, film quality, uniformity, etc.). Both technologies require major capital investment for industrial scale facilities. However, in each instance, choosing one technology over the other inevitably leads to a compromise on the overall product

performance and/or the optimisation of the manufacturing process. In order to reduce product cost and improve performance, there is a demand to improve upon the rate and, where applicable, the stability of the sputtering process, and a similar demand for improving/expanding the material choice and uniformity of the PECVD process to open up new applications. This work explores the potential of addressing these issues through the development of a hybrid system, which combines the latest magnetron sputtering technology, High Power Impulse Magnetron Sputtering (HiPIMS), with PECVD technology. It has been demonstrated by Fu *et al.,* that HiPIMS can be used successfully to enhance the deposition of carbon coatings via CVD route [15].

HiPIMS involves the application of very large power pulses to magnetron sputter cathodes for short periods. The peak pulse power can be in the megawatt range (with power densities of the order of 1 – 3 kW/cm^2), and the pulse duration is typically of the order of 80 – 160 μs, at repetition rates in the range of 10s to 100s of Hz. These intense pulses create peak electron densities in a plasma of 10^{18} to 10^{19} m^{-3} [16], leading to a high degree of ionization of the sputtered species (up to 90% depending on target material). This large ionization fraction of the sputtered target material is in contrast to conventional magnetron sputtering, where usually less than 1% of the sputtered material is ionized. The authors have demonstrated that the flux of highly ionised sputtered particles delivered to the growing film is highly dependent on the I – V characteristics at the target and the strength and degree of unbalance of the magnetic array in the magnetron [17]. For example, the data presented in this earlier work shows that the net deposition rate at the substrate is approximately halved as the B – field strength at the target is doubled. The control of this parameter, therefore, provides a route to decouple the flux of sputtered coating material arriving at the substrate and the density and temperature of the plasma generated in the CVD process zone. By strengthening the magnetic field and creating a balanced field (achieved through manipulation of the

magnets behind the target), the majority of the metal ions sputtered from the target will return to the target and never reach the substrate, but simultaneously a very high – density plasma will still be generated in the process zone. Adjustment of the magnetic array then allows a means of controlling the flux of sputtered metal dopant to the growing CVD film, whilst still operating at the same pressure and time averaged power and, therefore, still maintaining the same plasma density in the process zone.

Whilst hybrid systems have been demonstrated on the lab-scale, to date all examples have either relied on two plasma sources (e.g. pulsed DC for the magnetron and a RF bias on a static substrate to drive the CVD process), which imposes additional cost, or they have used one source and lacked any degree of process flexibility, because the PECVD process cannot be decoupled from the sputtering process. Each process has a region in the operating envelope where it dominates, meaning selection of film composition and other film/processing parameters is highly limited and may not be optimal. Utilising the HiPIMS power delivery mode to drive both the magnetron and the CVD process in the combined PVD – CVD system, with control of the flux of sputtered particles through the magnetic field strength at the target, offers a new means of process control in the hybrid system. Therefore, in this work the HiPIMS – CVD hybrid system is used to demonstrate a flexible deposition tool for functional films, such as transparent conductive oxides, and to overcome the limitations of each technique, such as for example low deposition rates under HiPIMS by controlling the magnetic field strength (B) at the target. Niobium doped titanium dioxide (Nb – TiO_2) has been selected to demonstrate coating deposition using a hybrid system, due to its interesting properties found in variety of applications. Due to its low resistivity of the order 10^{-4} Ωcm, high visible transparency of 90%, low cost and being non-toxic Nb – TiO_2 has been recently used as an Indium – free transparent conducting oxide (TCO) material [18] and as photo catalyst in the reduction of CO_2 to methanol [19, 20], in water purification or as a self-

cleaning coating for architectural glazing units [21, 22]. This work focuses to prove the concept of combining HiPIMS in adjustable magnetic field configuration with a CVD to deposit metal – doped compounds.

II. EXPERIMENTAL

Niobium – doped titanium dioxide (Nb – TiO_2) was deposited using a HiPIMS – CVD hybrid method. In this set up, the TiO_2 was deposited via a CVD route using volatile titanium (IV) tetraisopropoxide (TTIP, $Ti(OCH(CH_3)_2)$) as a precursor, without the addition of further oxygen co – reagent, which was necessary to maintain the operating pressure regime required for HiPIMS. The process was carried out in a vacuum chamber (L 320 mm, H 280 mm, D 280 mm), evacuated prior to deposition to the high vacuum range ~ $5x10^{-4}$ Pa. The substrate was mounted in front of the magnetron (distance ~100 mm) on a heated stage and the amount of TTIP introduced to the chamber was adjusted to give a constant chamber pressure. Argon gas was also introduced to strike the magnetron discharge. The Nb was sputtered directly from a 99.9% pure metal target (75 mm diameter) in the HiPIMS mode using a Chemfilt SINEX 3.0 power supply. FIG. 1 shows schematic drawing of the chamber set up.

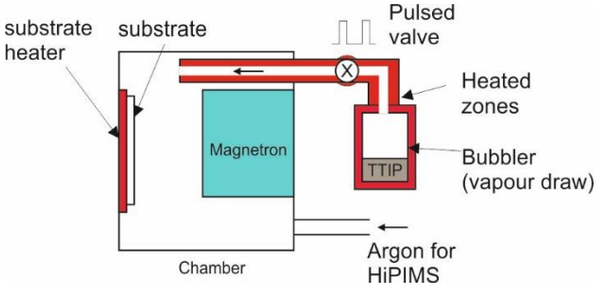

FIG. 1: Schematic drawing of hybrid HiPIMS – CVD system configuration.

The plasma discharge voltage was measured by an oscilloscope and is assumed to be equal to the potential dropped across the plasma. The average discharge power was

calculated from the HiPIMS current – voltage traces using Eq. (1) where V_p, I_p, Pw and f refer to the peak voltage, peak current, pulse width and frequency, respectively.

$$Power = V_p * I_p * Pw * f \quad (1)$$

The design of the magnetron allowed the degree of unbalance and magnetic field strength (and topology) above the racetrack to be varied by withdrawing or advancing the inner and outer pole pieces behind the target. This was done by adjusting Vernier screw gauges on the air – side of the VTech magnetron (Gencoa Ltd.). For these experiments, the degree of unbalance was kept constant and both inner and outer magnets were retracted together. Three positions were investigated, BF1 – BF3, with magnet positions and total B – field strength measured directly above the racetrack are shown in TABLE I. The strongest field is for the case BF1, with an intermediate field, BF2, and a considerably weaker field in BF3.

TABLE I: Magnetic pole positions and field strengths for configurations BF1, BF2 and BF3.

	Inner magnet spacing to target (mm)	Outer magnet spacing to target (mm)	B (kG) above the racetrack
BF1	12.5	12.5	1.62
BF2	15.5	15.5	1.10
BF3	20.5	20.5	0.54

Operating initially in PVD mode only, the Nb target was driven by the HiPIMS power supply over a range of possible parameters to determine stable operating conditions for this process. Parameters that were varied included time-averaged powers between 20 and 400 W, pulse frequencies in the range 50 – 500 Hz and pulse widths of 50 – 125 μs. The HiPIMS operating conditions used for coatings deposition are summarized in TABLE II.

TABLE II: Stable ranges of HiPIMS operating conditions identified for each magnetic configuration tested (Ar flow rates and operating pressures were kept constant for each configuration at 1 sccm and 1 Pa, respectively).

	HiPIMS conditions (no CVD)				
	Peak applied voltage (V)	Peak current (A)	Pulse frequency (Hz)	Pulse width (μs)	Average power (W)
BF1	520-612	11-42	100-200	80-100	59-285
BF2	440-522	10-28	100-200	80-100	70-258
BF3	479-660	7-18	100-200	80-100	46-95

During this stage of the work, the deposition rate of the sputtered Nb dopant was recorded using a quartz crystal monitor (QCM) and a Maxtor TM – 400 thickness monitor using density and impedance values for bulk niobium. The deposition rate of the Nb was controlled by adjusting the magnetic field strength, as described above, at each set of operating conditions.

Similarly, TiO_2 deposited via the CVD route from a TTIP volatile precursor was studied prior to combining with HiPIMS to form a hybrid method. It was important to find a range of CVD operating conditions that would provide high deposition rates, but still allow the pressure to be kept low enough to allow stable HiPIMS operation. Therefore, CVD deposition rates versus bubbler temperatures were studied, which are directly proportional to the precursor's vaporisation rate, i.e. amount of vapour allowed into the chamber during deposition, consequently dictating regimes of operating pressure during coating deposition. Normally, in CVD processes the vapour pressure of the liquid volatile precursor is chosen so that it is equal to that of water at 373 K, as shown in FIG. 2. The deposition rates and refractive indices of CVD TiO_2 films were modelled from ellipsometry measurements (J. A.

Woolam Co Ellipsometry Solutions). The ellipsometer was equipped with the Ellipsheer program, which allowed modelling of the film thickness from the detected change in polarization (ellipsometry measurement) of light of 632 nm wavelength passing through the sample under 70 ° angle of incidence. The refractive indices were calculated using the Sellmeier equation for transparent materials[23]:

$$n^2(\lambda) = A + \sum_{i=1}^{N_s} \frac{B_i \lambda^2}{\lambda^2 - C_i^2} \qquad (2)$$

where n is the refractive index, λ is the wavelength, and A, B_i and C_i are experimentally determined Sellmeier coefficients, and N_s is the number of non-constant Sellmeier coefficients.

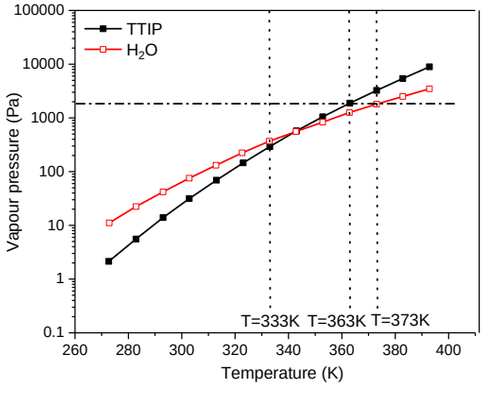

FIG. 2: Vapour pressure of TTIP and water as a function of temperature.

For the next stage of the work, when operating in hybrid mode, the CVD bubbler temperature was set to 60 °C, allowing precursor evaporation towards the chamber without creating excess vapour and increasing operating pressures above stable, controllable regimes for the HiPIMS process. In this arrangement, the HiPIMS driven Nb target was not only a source of dopant material in the deposited film, but also provided high – density plasma enhancement to the CVD process, allowing TiO_2 deposition at lower temperatures than in a conventional CVD process (the maximum substrate temperature during coating deposition

was 250 °C). TABLE III shows the operating conditions during Nb – TiO_2 thin film depositon using hybrid HiPIMS – CVD method.

TABLE III: Hybrid HiPIMS – CVD operating conditions identified for each magnetic configuration tested (operating pressure was kept constant at approx. 5 Pa).

	HiPIMS – CVD				
	Peak voltage (V)	Peak current (A)	Pulse frequency (Hz)	Pulse width (μs)	Ar flow rate (sccm)
BF1	550	10.0	100	125	0.8
BF2	490	4.7	100	125	1.2
BF3	510	4.0	100	125	0.8

The morphology of the as – deposited samples was characterised using scanning electron microscopy (SEM, Zeiss Supra 40VP), operating at an accelerating voltage of 4 keV, on the sample surface and fractured sections. The composition was quantified using energy – dispersive X – ray spectroscopy with a 40 mm^2 silicon drift detector (EDS, Trident™ system) operating at 7 keV. The signal was collected from the imaged area of approximately 100 μm^2 and the element concentrations in the sample was quantified using the ZAF correction. Low Energy Ion Scattering was used to measure the chemical composition of a thin film sample using a Qtac 100 instrument (ION – TOF GmbH). A 3 keV He+ primary ion source was used to measure the Nb, Ti, O, C and Si distributions using dynamic or sputter – depth profiling analysis. The crystal structure of the coatings was investigated using grazing angle X-ray diffractometry (GAXRD, PANalytical X'Pert – Pro). Samples were scanned from 20 to 80 $2\theta^o$ with a 0.02 $2\theta^o$ step size, under Cu Kα radiation at 1^o incident angle.

III. RESULTS AND DISCUSSION

As described in the Experimental section above, the Nb deposition rate was varied, at any given target power, by varying the magnetic field strength during HiPIMS deposition. FIG. 3 shows the deposition rates of the sputtered Nb, averaged per 100 W applied power, at pulse frequencies of 100 and 200 Hz (80 µs pulse width; 1 Pa pressure; 0.8 and 1.6% duty, respectively) measured in – situ using a quartz crystal monitor, as a function of magnetic field strength. These measurements were carried out without the presence of a CVD precursor.

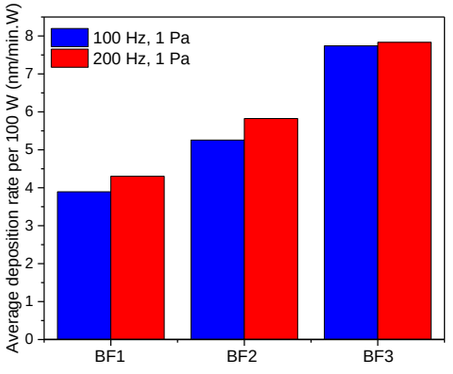

FIG. 3: Average power normalised deposition rates (nm/min per 100 W) of Nb for different magnetic field configurations BF1, BF2 and BF3 and pulse frequencies of 100 – 200 Hz at an operating pressure of 1 Pa.

Magnetic field strength weakens from left to right (BF1 to BF3) and as the field weakens the deposition rates progressively increase. In HiPIMS, as the magnetic field is reduced, the back attraction of metal ions to the target is reduced, allowing more ions to travel to the substrate and, thus, increasing the deposition rate [17, 24]. A marginally higher deposition rate was observed at 200 Hz pulse frequency, compared to 100 Hz, which is presumably due to the higher duty cycle at the higher frequency.

To optimise CVD deposition conditions, the deposition rates were studied as a function of bubbler temperature and temperature applied to the substrate holder. This approach was undertaken to find optimal conditions at the minimum vapour saturation in the

coating chamber, such that the HiPIMS and CVD processes could be merged at a later stage of this work. As expected, the operating pressure increased as the bubbler temperature was increased, which could be explained by Raoult's and Dalton's Laws: increasing the bubbler temperature raises the vapour pressure of the volatile TTIP and hence the chamber pressure, as shown in FIG. 4 a). FIG. 4 b) also shows the increase in deposition rates from 0.01 to 0.2 nm/min when the bubbler temperature increased from 45 to 60 ^{o}C.

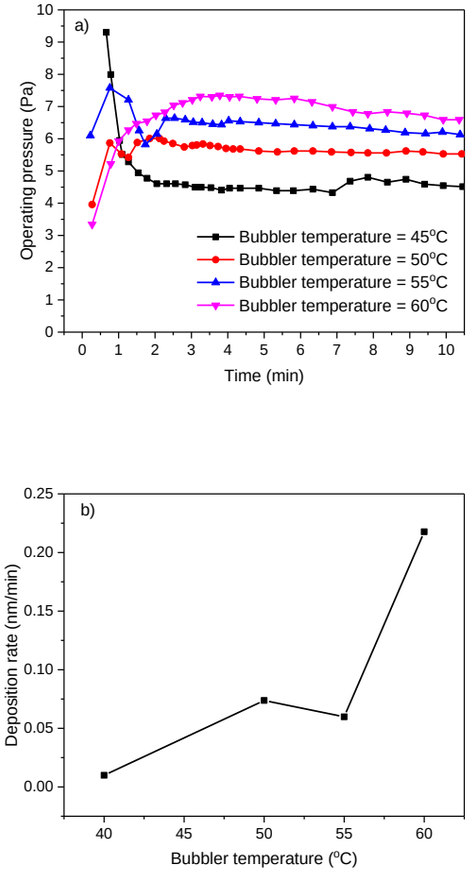

FIG. 4: Effect of the bubbler temperature on the chamber pressure during deposition a) and the deposition rate b) at substrate temperature of 200^{o}C.

Unsurprisingly, it was also observed that by increasing the substrate temperature (at a constant bubbler temperature) the deposition rate of the coating increased, which can be explained by the Arrhenius dependence indicating that surface reactions control the

deposition rates[25]. FIG. 5 shows that the deposition rate increased from 0.2 to 3.5 nm/min, as the substrate temperature increased from 200 to 325 °C, which also agrees with the literature[26]. Moreover, when increasing substrate temperature the refractive index also increased, which was most likely due to increased crystallinity of the deposited coatings or increased coating thickness, as suggested elsewhere[27, 28].

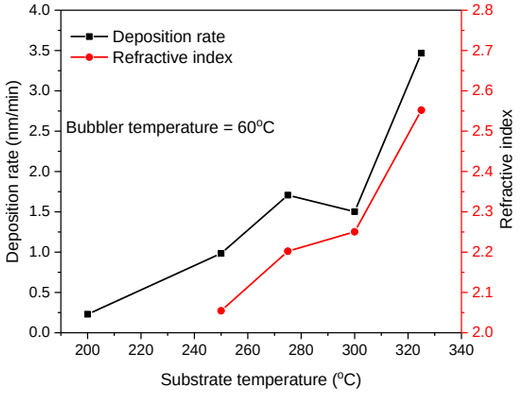

FIG. 5: Deposition rate and refractive index as a function of substrate temperature during the CVD process at bubbler temperature set to 60°C.

Having separately identified suitable HiPIMS and CVD operating parameters, trials were then performed to characterise the hybrid discharge behaviour to find stable control conditions for the combined process. It was found that the operating pressure proved to play a major role in merging the PECVD and HiPIMS processes together. From the CVD point of view an optimal operating pressures are higher, approximately > 27 Pa, than those for HiPIMS, which experiences severe arcing at pressures greater than approximately 5 Pa, thus compromising control. HiPIMS itself is a complex technique, which is inherently challenging to control and run allowing comparison between different systems. Plasma stability is affected by rarefaction of the argon gas and depends on pulse width, frequency and discharge voltage. To overcome this disparity of pressure regimes, the CVD process was run without any additional oxygen co – reagent. This approach was also adopted to minimise the

detrimental oxidation of the Nb sputter target. It has been reported that TiO_2 can be grown without oxygen from TTIP by plasma enhanced and remote plasma enhanced chemical vapour deposition [29]. This is because the precursor contains oxygen itself, which can be released by plasma decomposition, to react with the surface of the growing oxide film. However, it was also reported that higher levels of carbon contamination from the precursor was incorporated within the TiO_2 deposited if additional oxygen was not supplied to the reaction. Nevertheless, it will be shown from LEIS depth profiling analysis in a later stage of this section that no significant amount of carbon was found embedded in the coating.

Substrate temperature was also found to affect the hybrid process stability. FIG. 6 a) shows an example of hybrid HiPIMS-CVD process at a constant substrate temperature of 200 ^{o}C throughout the run. An operating pressure set to approx. 5 Pa and peak discharge current collected from oscilloscope are plotted as a function of deposition time. It can be seen that the process was stable throughout the operation time with some minor fluctuations of peak discharge current observed over the run time. FIG. 6 b) shows the evolution of the discharge current during a single pulse width (μs) collected using oscilloscope. The black curve shows the discharge current collected under standard HiPIMS operating procedures, before introducing CVD to the system. Blue and red curves show discharge currents during depositing Nb – TiO_2 in HiPIMS – CVD hybrid mode for 5 and 10 minutes, respectively. The only noticeable difference is before and after introducing the CVD precursor, which results in a steeper rise in current and a higher peak value. However, both processes can be controlled simultaneously throughout the deposition process.

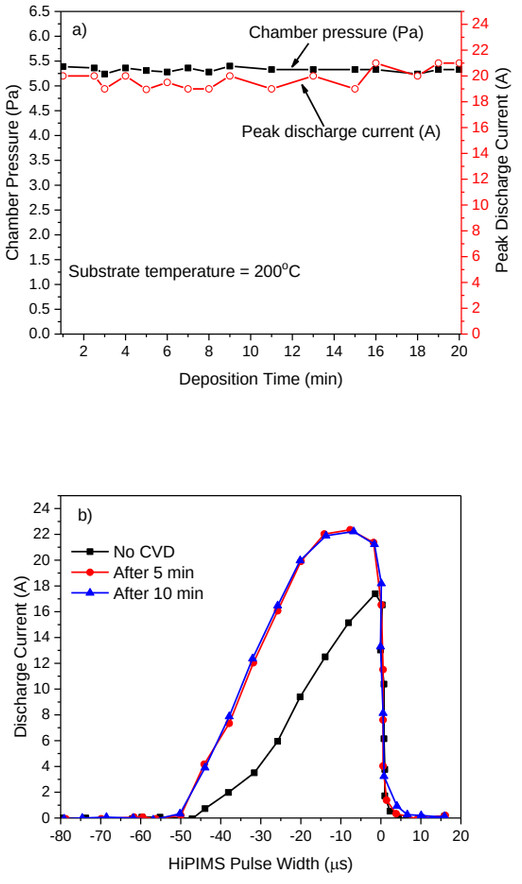

FIG. 6: Chamber pressure (monitored during the deposition using Baratron capacitance gauge) and peak plasma current (obtained from oscilloscope) as a function of time a) and peak current before HiPIMS and after 5 and 10 minutes of hybrid deposition b) of Nb – TiO_2 at substrate temperature set to 200 °C.

FIG. 7 a – b), in contrast, show the process operating at higher substrate temperature of 250 °C. The operating pressure was set again to approx. 5 Pa plotted along peak current values as a function of deposition time. In this case, gas partial pressures struggle to rich the targeted pressure of ~5 Pa at the beginning when the CVD process is introduced to the HiPIMS deposition and then stabilises after about 2 minutes of operation. The peak plasma current, on the other hand, gradually increases with time. This is especially visible in the discharge current graph (FIG. 7 b) where the peak current values doubled after introducing

the CVD precursor to the system (black curve shows discharge current of HiPIMS only at a single pulse before CVD was introduced to the system, whereas red curve shows the discharge current at hybrid HiPIMS – CVD operation after 2 minutes). Moreover, after additional 5 minutes of operation the discharge current increased again (blue curve in FIG. 7 b) implying instability in the plasma operation under selected conditions. One plausible cause of this phenomenon may be that the increased substrate temperature on the substrate holder causes the TTIP precursor to become more volatile. This in turn is poisoning the target surface and the plasma is reaching overcurrent flows seen in gradual increase in peak current discharge recorded over deposition time. Consequently, this could lead to HiPIMS plasma arc, instability and loss of discharge. However, more work needs to be done to confirm this statement.

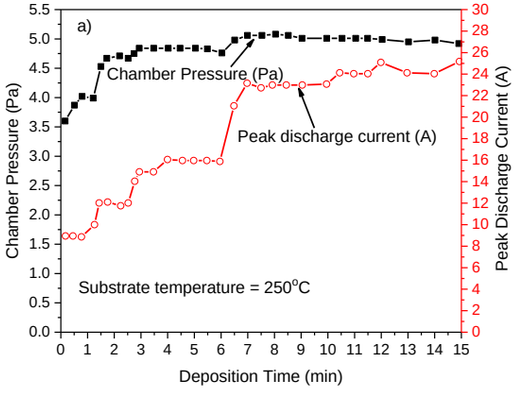

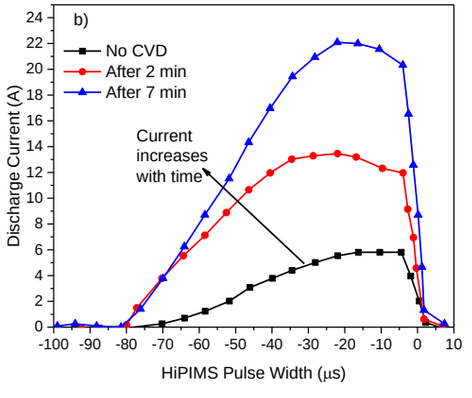

FIG. 7: Chamber pressure (monitored during the deposition using Baratron capacitance gauge) and peak plasma current (obtained from oscilloscope) plotted as a function of time a) and peak current before HiPIMS and after 2 and 7 minutes of hybrid deposition b) of Nb – TiO_2 at substrate temperature set to 250 ^oC.

The morphology of the Nb – TiO_2 coatings deposited by hybrid HiPIMS – CVD method are shown in FIG. 8 a – c) and the pictures show coatings deposited at the weakest magnetic field configurations, which lead to deposition of the thickest coatings. The coating's top surface appear fully dense and relatively smooth with some larger grains visible at higher magnification image in FIG. 8 b). Cross-sectional image in FIG. 8 c) shows that the coating thickness is about 550 nm and that the coating is indeed dense throughout its thickness, without noticeable larger pores or voids. It is not possible to independently verify the PECVD deposition rate in the hybrid system as a single plasma source drives both sources of deposited material.

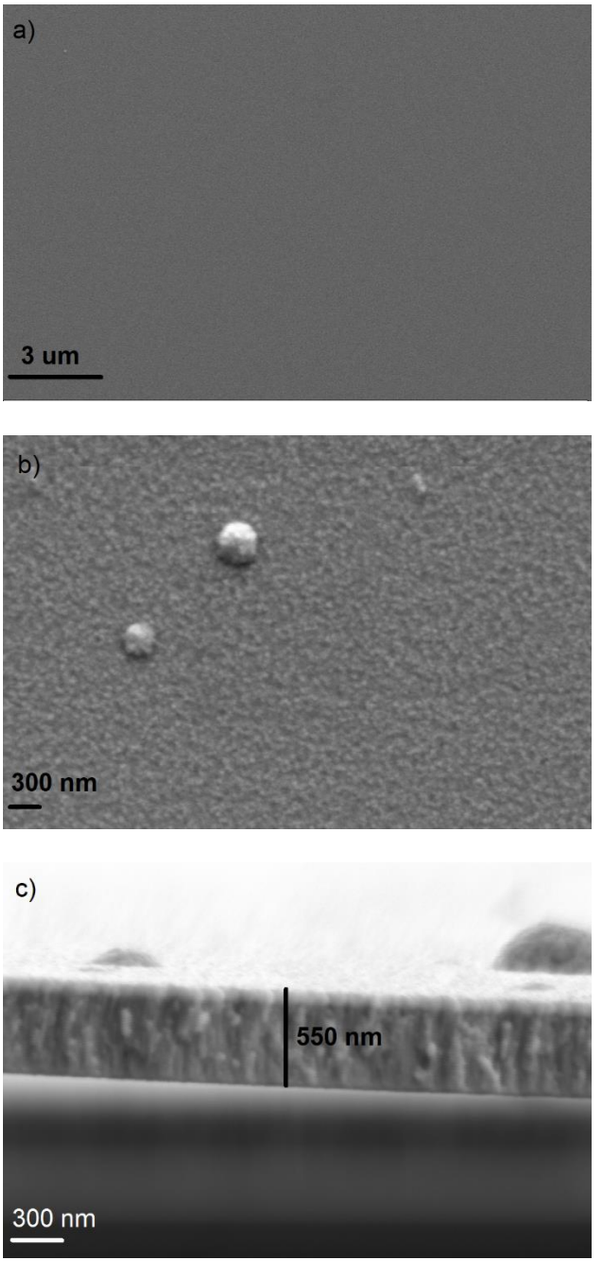

FIG. 8: SEM images of Nb – TiO_2 hybrid coatings collected from the surfaces a – b) under 15k and 50k magnification, respectively, and cross-section collected under 85k magnification c) samples deposited in hybrid HiPIMS – CVD process.

The coatings were then analysed by EDS to quantify the composition of the films. EDS data was collected at low acceleration energy (7 keV) to avoid a significant contribution from the underlying substrate material. The signal picked up from the *Nb L* and *Ti K* lines was then collected and quantified using the ZAF correction, as shown in TABLE IV. In

agreement with the deposition rate measurements collected from HiPIMS deposition under variable magnetic field strength (see FIG. 2), the atomic concentration of Nb is lower in the samples deposited at the strongest magnetic field configurations and increases as the field strength weakens. This phenomenon results from a greater number of the metal ions sputtered from the target returning to the target and never reaching the substrate at strong magnetic field configurations and therefore, less Nb being deposited [17, 24]. At weaker magnetic fields, on the other hand, the ions are able to escape the magnetic trap in front of the target and the Nb content in the film is much greater (up to 11% in these tests). The relatively large increase in Nb content with weakening field strength in the hybrid films, compared to the differences in deposition rate measured for Nb only films in HiPIMS mode may possibly arise from poisoning of the Nb target by the TTIP precursor at the lower target sputtering rates. However, further investigations are needed to confirm this suggestion.

TABLE IV: Atomic concentration of elements detected in Nb – doped TiO_2 deposited in hybrid HiPIMS – CVD mode and measured by EDS.

Magnetic field strength (B)	O K (at %)	Ti K (at %)	Nb L (at %)
BF1	61.0	35.5	3.5
BF2	64.2	31.5	4.3
BF3	68.9	20.1	11.1

To compare the thickness of Nb – doped TiO_2 films at the strongest (BF1) and the weakest (BF3) magnetic fields, coatings were analysed using depth profiling Low Energy Ion Scattering. FIG. 9 a – b) shows the chemical composition of Ti, Nb, O and Si ions. There is a significant difference in compositions obtained from LEIS and EDS analysis, which is related to differences in sensitivity of the analytical techniques used and could potentially indicate some variations in coating uniformity (not uncommon in CVD processes) across a larger

surface area than that submitted to each analysis. Nevertheless, the trend in the amount of Nb doped into the CVD deposited TiO_2 coating from HiPIMS under variable magnetic field strength are in agreement between both techniques. Moreover, there is no carbon detected within the film across its thickness indicating that the carbon content was < 1 at% even though TiO_2 was deposited from TTIP precursor without additional O_2 gas flow introduced to the chamber, as mentioned above.

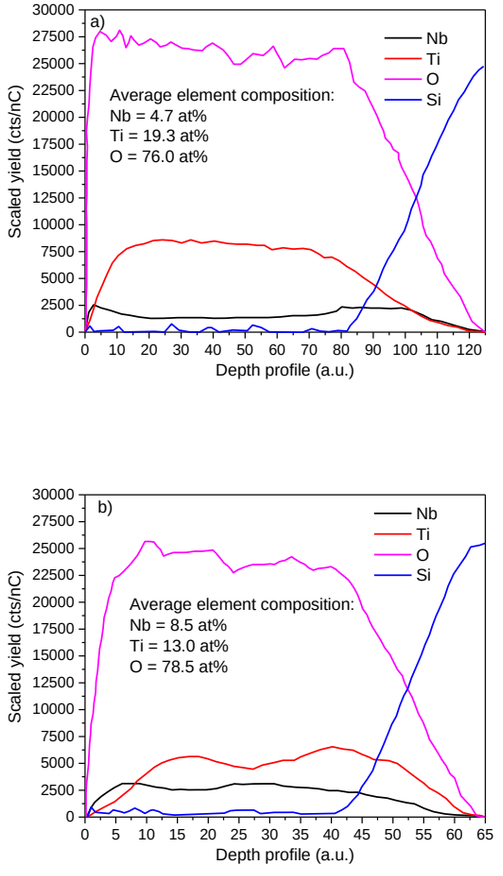

FIG. 9: Through film thickness distributions of oxygen, titanium and niobium measured by Low Energy Ion Scattering (LEIS) at the strongest, BF1 a) and the weakest, BF3 b) magnetic fields. Any carbon contamination was undetectable. The increase in silicon substrate signal shows the film interface.

As-deposited samples were also investigated by GAXRD at an incidence angle of 1 º. The analysis confirmed differences in the coatings' structures that were deposited at different magnetic field configurations. FIG. 10 shows XRD spectra for the coated samples and a Si wafer reference. Peaks have not been de-convoluted and characteristic peaks were assigned using diffraction patterns reported in ICDD. FIG. 10 reveals the evolution of the Nb – TiO_2 phases from amorphous thin films at BF1, deposited under the strongest magnetic field configuration through weakly crystalline, possibly highly – textured nanocrystalline monoclinic Nb_2O_5 (m-Nb_2O_5, JCPDS 80-2493), as it has been demonstrated that in thin films unlike the bulk materials higher symmetry phases could form at lower temperatures [30]. However, it is likely that the peak at 25.3º 2θ angle comes from (101) anatase TiO_2 phase (*A*-TiO_2, JCPDS 84-1286) and no crystal phases of niobium dioxide have been detected under BF2 configuration. At BF3 configuration, on the other hand, a pseudo – hexagonal (*TT*-Nb_2O_5, JCPDS 28-0317) and/or orthorhombic (*T*-Nb_2O_5, JCPDS 30-0873) phases of Nb_2O_5 could be seen. Due to the similarity of the diffraction patterns for pseudo – hexagonal and orthorhombic Nb_2O_5 phases it was not possible to distinguish between them [31], however it is clearly seen that Nb doped into CVD TiO_2 from the metallic target sputtered under HiPIMS mode undergoes competitive oxidation forming Nb_2O_5 within amorphous TiO_2 matrix. This could suggest that above 10 at% of Nb doped into TiO_2 matrix it forms nanocomposite Nb_2O_5 phases dispersed in the amorphous TiO_2 matrix. Nevertheless, to confirm that claim further HRTEM analysis is necessary.

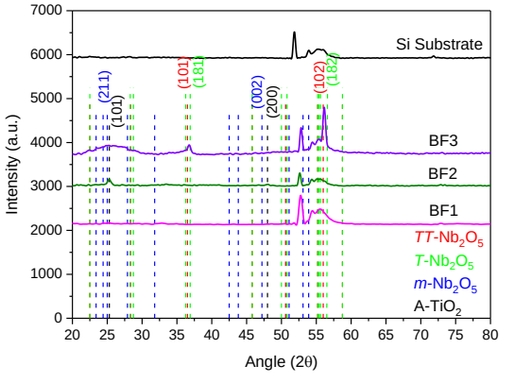

FIG.10 XRD spectra collected from uncoated Si wafer substrate and Nb – TiO_2 coatings deposited under variable magnetic field strengths.

IV. SUMMARY AND CONCLUSIONS

A hybrid HiPIMS – CVD deposition system has been developed and demonstrated through the deposition of Nb – TiO_2 coatings. The plasma generated by the HiPIMS source also drives the CVD precursor decomposition and reaction chemistry. The deposition rate and, therefore, the proportion of Nb in the resulting coatings characterised in this work is controlled by varying the magnetic field strength in the magnetron, at each set of operating conditions. This, in turn, is achieved by physically moving the inner and outer magnetic arrays with a Vernier screw. The deposited films were smooth and dense, with Nb contents ranging from approximately 3.5 at% to 11.1 at%. Film structures varied from an amorphous through possibly 2-phase consisting of anatase titania and Nb_2O_5, to coatings containing Nb – dominant phases with no crystalline titania detected. The main challenges in operating the hybrid system were related to HiPIMS stability at higher pressure ranges and elevated process temperatures, indicating that there appears to be only a narrow process window in which the HiPIMS – PECVD system can be successfully operated. Nevertheless, this work demonstrates that the two processes can be operated simultaneously with only one power

supply driving both discharges and that magnetron field strength can be used as a control parameter for film composition.

ACKNOWLEDGMENTS

This work was supported by EPSRC under the grant number EP/N031717/1.

REFERENCES

[1]D. Benetti, Nouar, R., Nechache, R., Pepin, H., Sarkissian, A., Rosei, F., MacLeod, J. M., Scientific Reports **7** (2503), 1-9 (2017).
[2]M. Novotný, Jelínek, M., Bulíř, J., Lančok, J., Vorlíček, V., Bonarski J., Applied Physics A **79** (4-6), 1267–1270 (2004).
[3]X. X. Xi, Pogrebnyakov, A. V., Xu, S. Y., Chen, K., Cui, Y., Maertz, E. C., Zhuang, C. G., Li, Q., Lambord, D. R., Redwing, J. M., Liu, Z. K., Soukiassian, A., Schlom, D. G., Weng, X. J., Dickey, E. C., Chen, Y. B., Tian, W., Pan, X. Q., Cybart, S. A., Dynes, R. C., Physica C **456**, 22-37 (2007).
[4]C. Schaefer, Brauer, G., Szczyrbowski, J. , Surf. Coat. Technol. **93**, 37-45 (1997).
[5]M. C. Vasudev, Anderson, K. D., Bunning, T. J., Tsukruk, V. V., Naik, R. R., ACS Appl. Mater. Inetrfaces **5**, 3983-3994 (2013).
[6]T. Takeno, Abe, S., Adachi, K., Miki H., Takagi, T., Diamond & Related Materials **19**, 548-552 (2010).
[7]N. Li, Ruzic, D. N., Powell, R. A., J of Vac. Sci Technol. B **22** (6), 2734-2742 (2004).
[8]K. L. Kolipaka, Brueser, V., Schlueter, R., Quade, A., Schaefer, J., Wulff, H., Strunskus, T., Faupel, F., Surf Coat Technol. **207**, 565-570 (2012).
[9]J. W. Miller, Khatami, Z., Wojcik, J., Bradley, J. D. B., Mascher, P., Surf Coat Technol. **336**, 99-105 (2018).
[10]R. Žemlička, Jílek, M., Vogl, P., Šrámek, J., Souček, P., Buršíková, V., Vašina, P., Surf Coat Technol. **304**, 9-15 (2016).
[11]c. T. Guo, Dittrich, K.-H., Appl. Surf. Sci. **253**, 4935-4941 (2007).
[12]J. F. Chang, Ueng, H. Y., Young, T. F., Wang, Y. C., Hwang, W. C., Surf Coat Technol. **157**, 179-184 (2002).
[13]M.-G. Tsaia, Huang, M.-S., Chen, L.-K., Shen, Y.-D., Lin, M.-H., Chiang, Y.-C., Ou, K.-L., Ou, S.-F., Ceramics Int. **39**, 8335-8340 (2013).
[14]W. Yang, Ke, P., Fang, Y., Zheng, H., Wang, A., Appl. Surf. Sci. **270**, 519-525 (2013).
[15]Q. Fu, Lundin, D., Nicolescu, C. M., J. of Mat Eng and Perform **23** (2), 506-517 (2014).
[16]J. T. Gudmundsson, Brenning, N., Lundin, D., Helmersson, U., J. Vac. Sci. Technol. A **30** (3), 030801-1030801-1030834 (2012).
[17]J. W. Bradley, Mishra, A., Kelly, P. J., J. Phys. D: Appl. Phys. **48** (2015).
[18]K. Safeen, Micheli, V., Bartali, R., Gottardi, G., Safeen, A., Ullah, H., Laidani, N., Mat Sci in Semicond Process **66** (2017).
[19]M. V. Nogueira, Lustosa, G. M. M. M., Kobayakawa, Y., Kogler, W., Ruiz, M., Monteiro Filho,E. S., Zaghete, M. A., Perazolli, L. A., Advances in Mat Sci and Eng **2018**, 1-8 (2018).
[20]J. Kiwi, Suss, J. T., Szapiro, S., Chem. Phys. Letts. **106** (1-2), 135-138 (1984).
[21]L. da Silva, F., Avansi Jr, W., Catto, A. C., Rodrigues, J. E. F. S., Bernardi, M. I. B., Mastelaro, V. R., Photocal **215**, 1800321 (1800328) (2018).
[22]X. Yang, Min, Y., Li, S., Wang, D., Mei, Z., Liang, J., Pan, F., Cat Sci & Technol **8**, 1357-1365 (2018).
[23]Y. Fang, Furniss, D., Jayasuriya, D., Parnell, H., Tang, Z. Q., Gibson, D., Bayya, S., Sanghera, J., Seddon, A. B., Benson, T. M., Optical Materials: X **2**, 100030 (2019).

[24]A. Mishra, Kelly, P. J., Bradley, J. W., Plasma Sources Sci. Technol. **19** (2010).
[25]G. A. Battiston, Gerbasi, R., Gregori, A., Porchia, M., Cattarin, S., Rizzi, G.A., Thin Solid Films **371**, 126-131 (2000).
[26]H. Chiba, Tada, K.-i., Yamamoto, T., Iwanaga, K., MRS Online Proceedings Library Archive **1288** (2011).
[27]C. Jiménez, De Barros, D., Darraz, A., Deschanvres, J.-L., Rapenne, L., Chaudouët, P., Méndez, J. E., Weiss, F., Thomachot, M., Sindzingre, T., Berthomé, G., Ferrer, F. J., Surf Coat Technol. **201**, 8971-8975 (2007).
[28]Y. Takahashi, Suzuki, H., Nasu, M. , J. Chem. Soc., Furaday Trans. 1 **81**, 3117-3125 (1985).
[29]H. Nizard, Kosinova, M. L., Fainer, N. I., Rumyantsev, Yu. M., Ayupov, B. M., Shubin, Yu. V., Surf Coat Technol. **202**, 4076-4085 (2008).
[30]V. A. Logacheva, Divakova, N. A., Tikhonova, Y. A., Dolgopolova, E. A., Khoviv, A. M, Inorganic Materials **43**, 1230-1234 (2007).
[31]R. Fiz, Appel, L., Gutiérrez-Pardo, A., Ramírez-Rico, J., Mathur, S., ACS Appl. Mater. Inetrfaces **8**, 21423−21430 (2016).

TABLES

TABLE I: Magnetic pole positions and field strengths for configurations BF1, BF2 and BF3.

TABLE II: Stable ranges of HiPIMS operating conditions identified for each magnetic configuration tested (Ar flow rates and operating pressures were kept constant for each configuration at 1 sccm and 1Pa, respectively).

TABLE III: Hybrid HiPIMS – CVD operating conditions identified for each magnetic configuration tested (operating pressure was kept constant at approx. 5 Pa).

TABLE IV: Atomic concentration of elements detected in Nb – doped TiO_2 deposited in hybrid HiPIMS – CVD mode and measured by EDS.

FIGURE CAPTIONS

FIG. 1: Schematic drawing of hybrid HiPIMS – CVD system configuration.

FIG. 2: Vapour pressure of TTIP and water as a function of temperature.

FIG.3: Average power normalised deposition rates (nm/min per 100 W) of Nb for different magnetic field configurations BF1, BF2 and BF3 and pulse frequencies of 100 – 200 Hz at an operating pressure of 1 Pa.

FIG. 4: Effect of the bubbler temperature and the chamber pressure during deposition a) and the deposition rate b) at substrate temperature of 200 ^{o}C.

FIG. 5: Deposition rate and refractive index as a function of substrate temperature during the CVD process at bubbler temperature set to 60 ^{o}C.

FIG. 6: Chamber pressure (monitored during the deposition using Baratron capacitance gauge) and peak plasma current (obtained from oscilloscope) plotted as a function of time a) and peak current before HiPIMS and after 5 and 10 minutes of hybrid deposition b) of Nb – TiO_2 at substrate temperature set to 200 ^{o}C.

FIG. 7: Chamber pressure (monitored during the deposition using Baratron capacitance gauge) and peak plasma current (obtained from oscilloscope) plotted as a function of time a) and peak current before HiPIMS and after 2 and 7 minutes of hybrid deposition(b) of Nb – TiO_2 at substrate temperature set to 250 ^{o}C.

FIG. 8: SEM images of Nb – TiO_2 hybrid coatings collected from the surfaces a – b) under 15k and 50 k magnification, respectively, and cross – section collected under 85k magnification c) samples deposited in hybrid HiPIMS – CVD process.

FIG. 9: Through film thickness distributions of oxygen, titanium and niobium measured by Low Energy Ion Scattering (LEIS) at the strongest, BF1 a) and the weakest, BF3 b) magnetic fields. Any carbon contamination was undetectable. The increase in silicon substrate signal shows the film interface.

FIG. 10: XRD spectra collected from uncoated Si wafer substrate and Nb – TiO_2 coatings deposited under variable magnetic field strengths.

Journal of Vacuum Science Technology A

PLEASE CITE THIS ARTICLE AS DOI: 10.1116/6.0000118

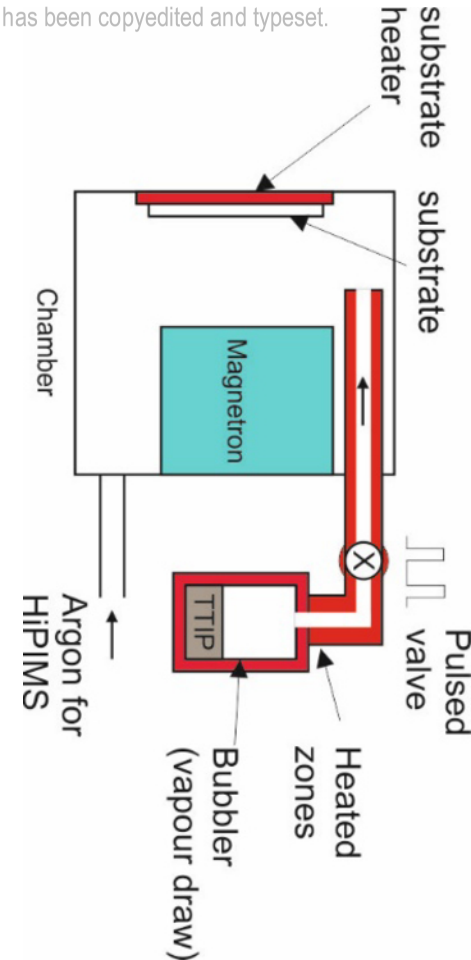

Journal of Vacuum Science Technology A

PLEASE CITE THIS ARTICLE AS DOI: 10.1116/6.0000118

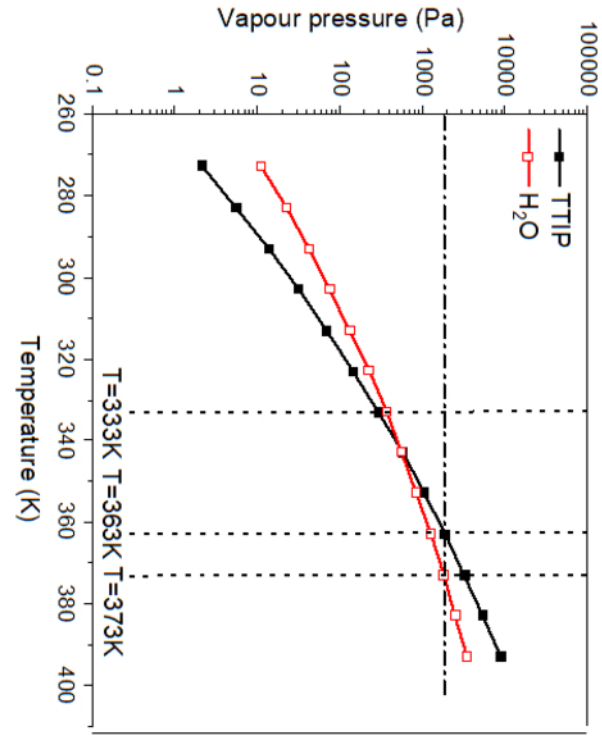

Journal of Vacuum Science Technology A

PLEASE CITE THIS ARTICLE AS DOI: 10.1116/6.0000118

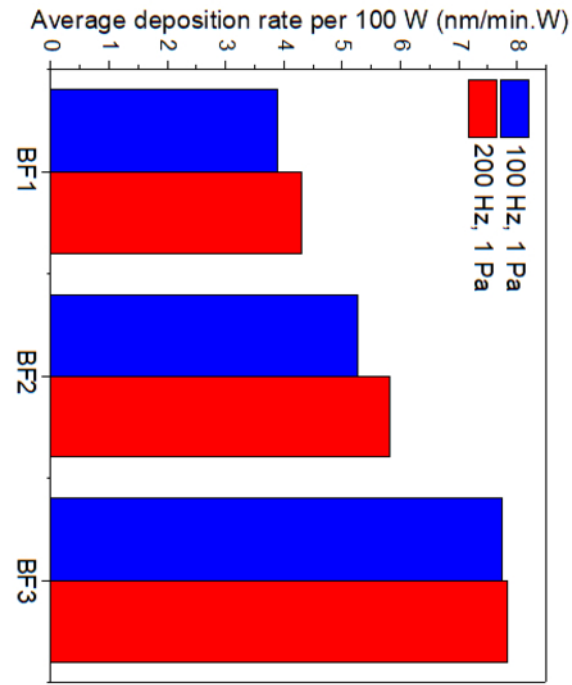

Journal of Vacuum Science Technology A

PLEASE CITE THIS ARTICLE AS DOI: 10.1116/6.0000118

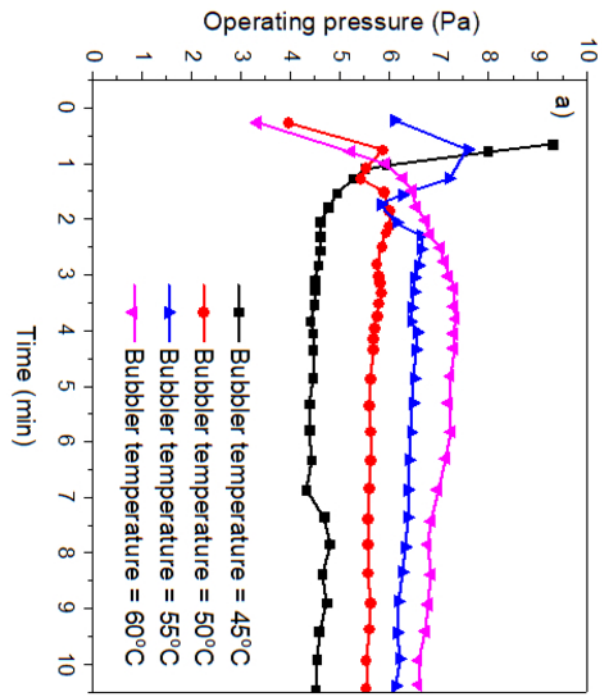

Journal of Vacuum Science Technology A

PLEASE CITE THIS ARTICLE AS DOI: 10.1116/6.0000118

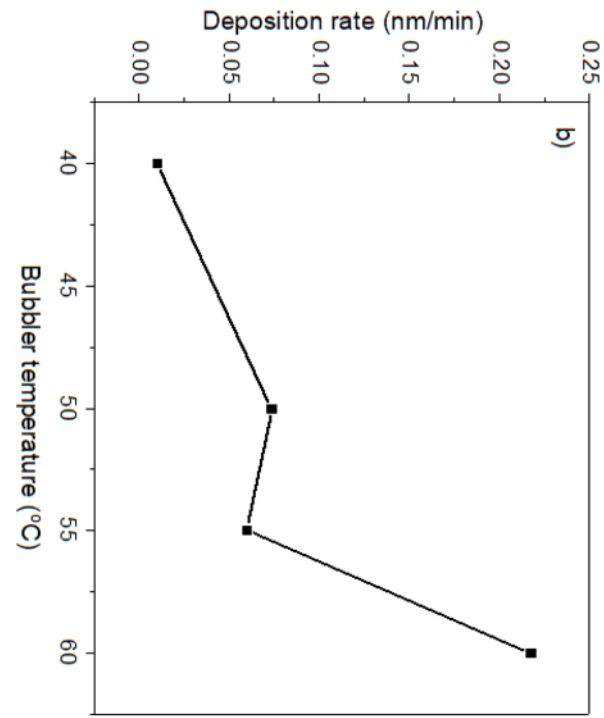

Journal of Vacuum Science Technology A

PLEASE CITE THIS ARTICLE AS DOI: 10.1116/6.0000118

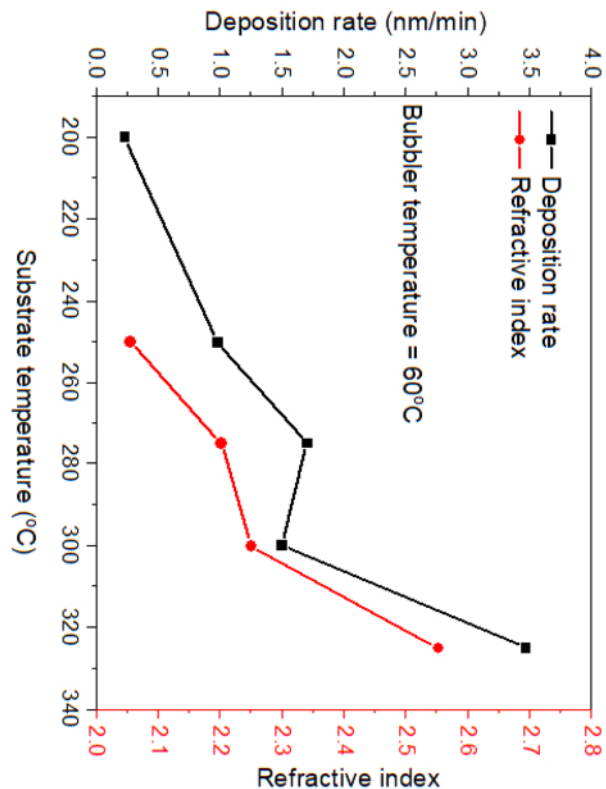

Journal of Vacuum Science Technology A

PLEASE CITE THIS ARTICLE AS DOI: 10.1116/6.0000118

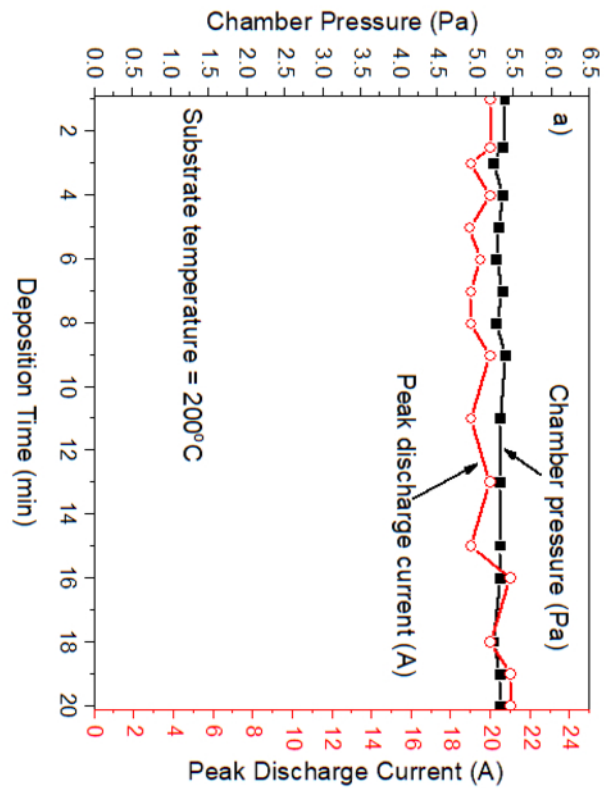

Journal of Vacuum Science Technology A

PLEASE CITE THIS ARTICLE AS DOI: 10.1116/6.0000118

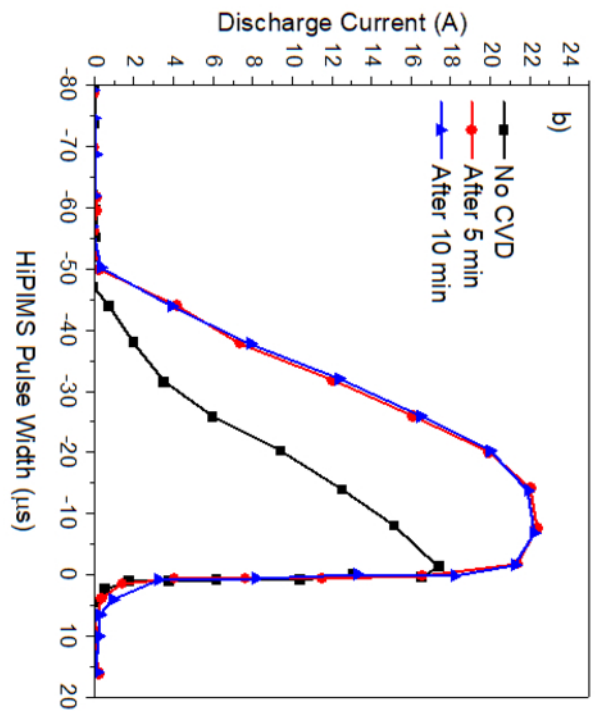

Journal of Vacuum Science Technology A

PLEASE CITE THIS ARTICLE AS DOI: 10.1116/6.0000118

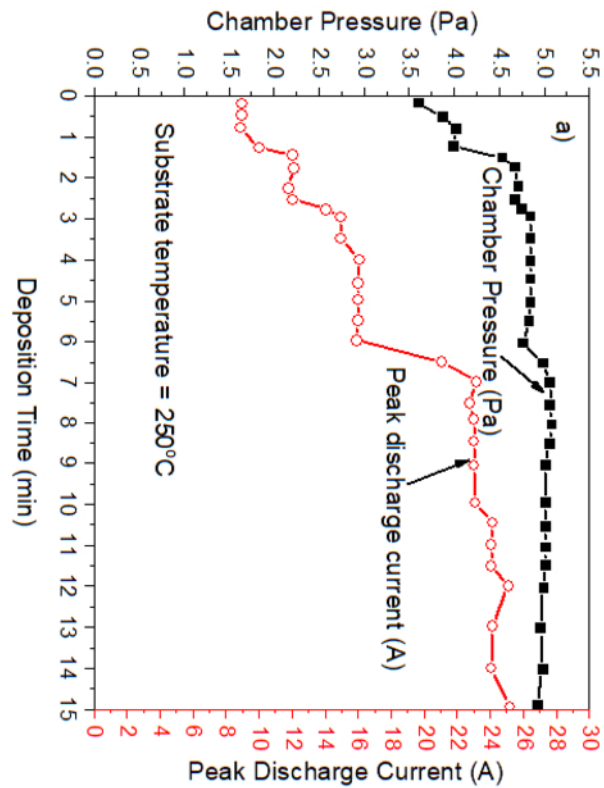

Journal of Vacuum Science Technology A

PLEASE CITE THIS ARTICLE AS DOI: 10.1116/6.0000118

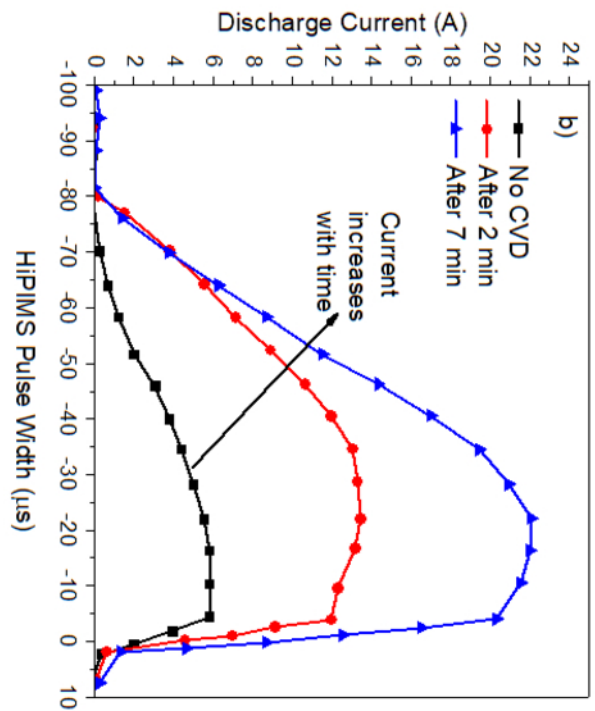

Journal of Vacuum Science Technology A

PLEASE CITE THIS ARTICLE AS DOI: 10.1116/6.0000118

Journal of Vacuum Science Technology A

PLEASE CITE THIS ARTICLE AS DOI: 10.1116/6.0000118

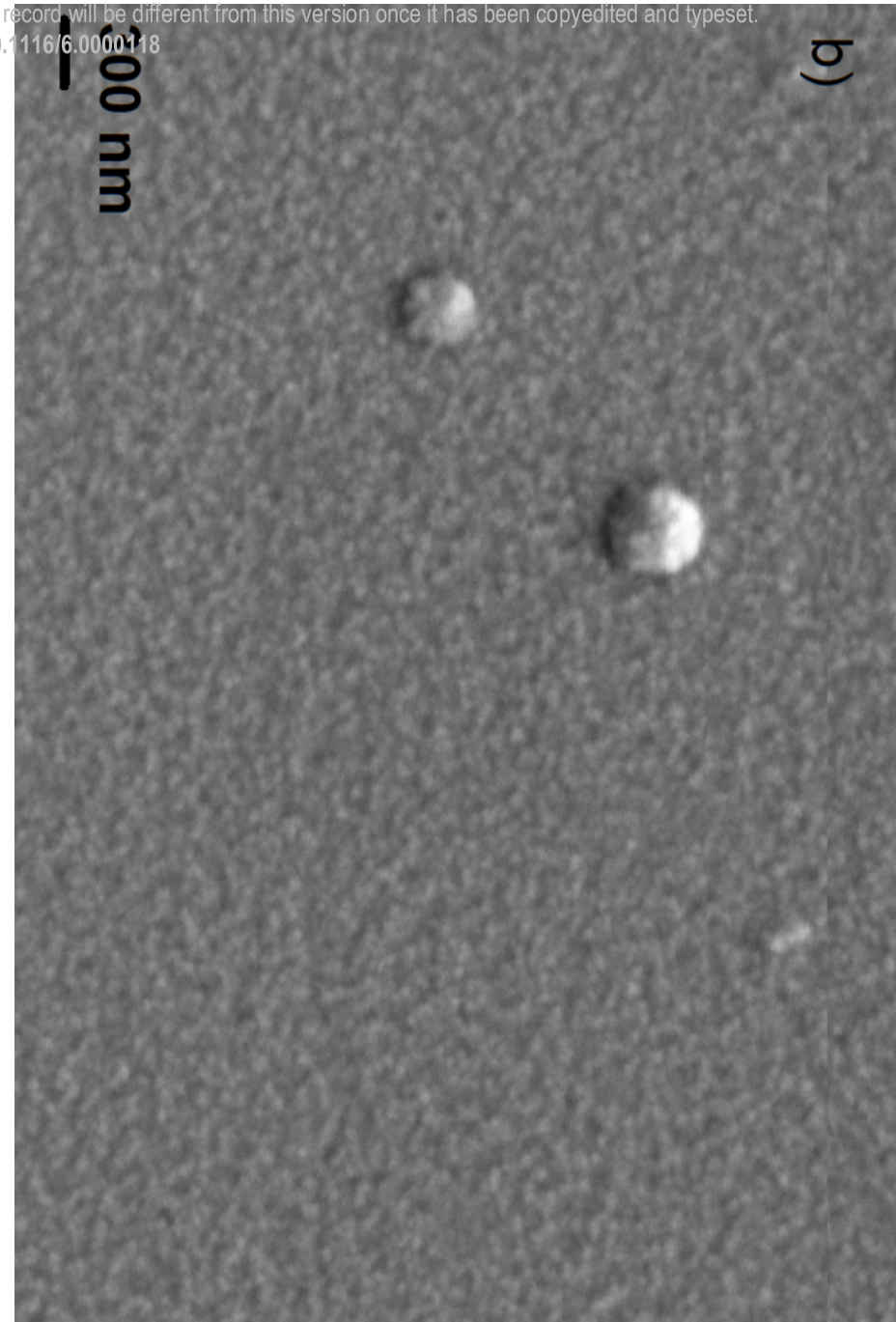

Journal of Vacuum Science Technology A

PLEASE CITE THIS ARTICLE AS DOI: 10.1116/6.0000118

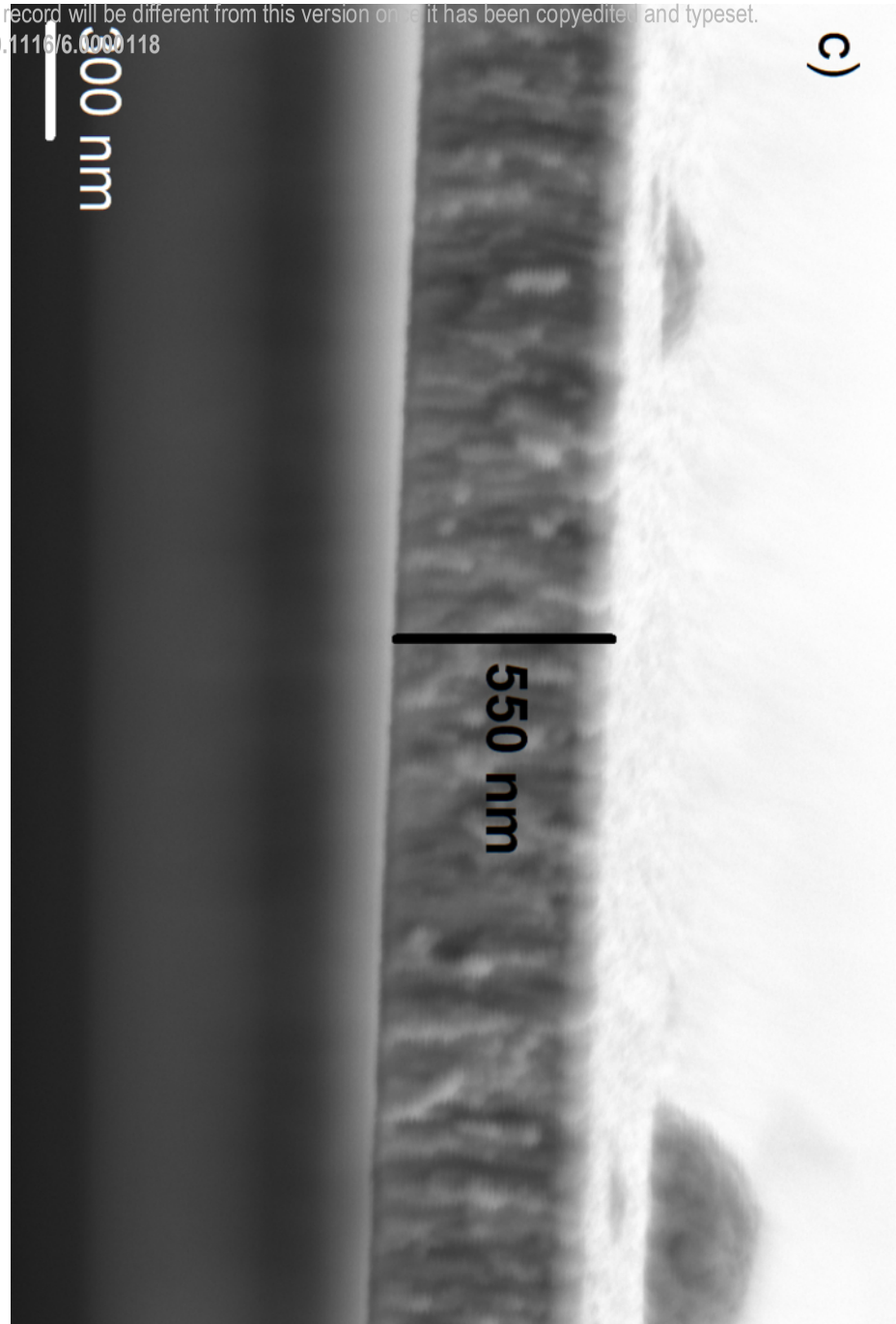

Journal of Vacuum Science Technology A

PLEASE CITE THIS ARTICLE AS DOI: 10.1116/6.0000118

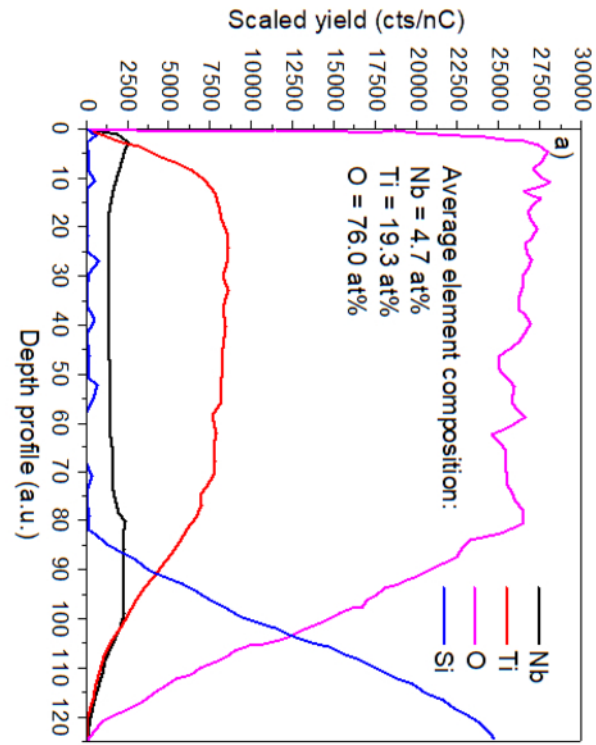

Journal of Vacuum Science Technology A

PLEASE CITE THIS ARTICLE AS DOI: 10.1116/6.0000118

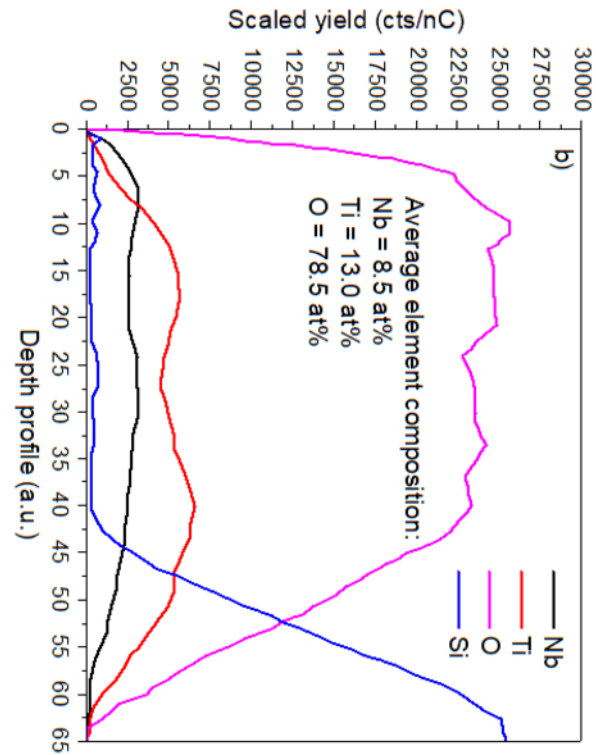

Journal of Vacuum Science Technology A

PLEASE CITE THIS ARTICLE AS DOI: 10.1116/6.0000118